


Article

# Water-Assisted Catalytic VACNT Growth Optimization for Speed and Height

Karlheinz Strobl<sup>1</sup> and Fahd Rajab<sup>2,\*</sup> 

<sup>1</sup> CVD Equipment Corporation, 355 S. Technology Drive, Central Islip, NY 11722, USA; kstrobl@cvdequipment.com

<sup>2</sup> Chemical Engineering Department, Najran University, Najran 11001, Saudi Arabia

\* Correspondence: fahdrajab7@gmail.com or fmrajab@nu.edu.sa; Tel.: +966-175428942

**Abstract:** The super-growth approach for carbon nanotubes synthesis is frequently used to boost the growth rate, catalyst lifespan, and height of vertically aligned carbon nanotubes. The elimination of amorphous carbon from catalyst particles, commonly made of iron, by injecting water vapor into a chemical vapor deposition process can enhance the purity, alignment, and height of carbon nanotubes and prevent the partial oxidation of the metallic catalyst. We present the development of a modified growth-optimized water-assisted super-growth vertically aligned carbon nanotube process by optimizing the catalyst layer structure and water vapor concentration for a carbon nanotube growth process for 4" diameter Si wafers. A significant finding is that under optimized water-assisted growth conditions over 4 mm, highly uniform tall, vertically aligned carbon nanotube structures can be grown with a minimum top crust layer of about ~5–10  $\mu\text{m}$  thickness. This was achieved with a catalyst film comprising a >400 nm thermal  $\text{SiO}_2$  layer on top of a 4" diameter Si wafer that was overcoated with an e-beam batch process run that first deposited a 20 nm  $\text{SiO}_2$  layer, a 10 nm  $\text{Al}_2\text{O}_3$  layer, and a 1.1 nm Fe layer, in a 4-h growth process step.

**Keywords:** VACNT; CVD;  $\text{Al}_2\text{O}_3$  buffer layer; water vapor; super-growth



**Citation:** Strobl, K.; Rajab, F. Water-Assisted Catalytic VACNT Growth Optimization for Speed and Height. *Processes* **2023**, *11*, 1587. <https://doi.org/10.3390/pr11061587>

Academic Editor: Andrea Petrella

Received: 16 April 2023

Revised: 4 May 2023

Accepted: 12 May 2023

Published: 23 May 2023



**Copyright:** © 2023 by the authors. Licensee MDPI, Basel, Switzerland. This article is an open access article distributed under the terms and conditions of the Creative Commons Attribution (CC BY) license (<https://creativecommons.org/licenses/by/4.0/>).

## 1. Introduction

Carbon nanotubes (CNTs) have been the focus of research in recent decades due to their unique electronic and mechanical properties [1,2]. Their properties have been utilized to improve various applications, such as steam generation, water splitting, supercapacitors, as well as desalination, water vapor condensation [3–8], and blood oxygenation. The integration of CNTs in any application requires the control of their synthesis method for yield, alignment, and purity [9]. CNTs can be synthesized using arc discharge, laser ablation, high-pressure carbon monoxide disproportionation (Hipco), and chemical vapor deposition (CVD) [10,11]. In the CVD process, the thermal decomposition of hydrocarbon vapor is achieved in the presence of a metal catalyst [12–14]. Synthesis by CVD enables control of the properties and aspect ratio of vertically aligned multi-walled carbon nanotubes (VACNTs). Since its introduction in 2004 by Hata et al. [15],  $\text{H}_2\text{O}$  vapor-assisted VACNT growth, commonly known as the super-growth method for CNT synthesis, has been used to increase the growth rate, catalyst lifetime, and height of VACNTs. Adding water vapor to the CVD process can improve the CNT purity, alignment, and growth height by removing amorphous carbon on the (typically Fe) catalyst particles owing to the partial oxidation of the metallic catalyst [12,15–17]. Most related studies that used sputtered  $\text{Al}_2\text{O}_3$  reported that the atomic layer deposition (ALD) nm-thick thin film deposition of  $\text{Al}_2\text{O}_3$  was not as effective for tall VACNT growth. The  $\text{Al}_2\text{O}_3$  morphology resulting from thin-film deposition significantly affects a catalyst's lifetime [18].

The mechanism and kinetics of VACNT growth have been studied extensively [19]. The VACNT growth mechanism has been identified as a tip growth mechanism where

catalyst–substrate interaction is weak and hydrocarbon decomposes on the top surface of the metal, allowing carbon to diffuse through the metal catalyst, so CNT precipitates out across the metal bottom, displacing the entire catalyst particle from the substrate. CNT continues to grow vertically as long as the top of the metal is accessible for new hydrocarbon breakdown. Once the metal is completely coated with excess carbon, its catalytic activity decreases, and CNT growth ceases [19–21]. Cao et al. found the optimum concentration of the  $\text{Fe}_3\text{O}_4$  catalyst for the maximum VACNT thickness, which showed a six-fold increase in growth with the addition of water vapor [12]. By partially oxidizing the metal catalyst, adding water vapor to the CVD process removes amorphous carbon from the catalyst, which improves the purity and growth of CNTs [15,22]. The effect of the  $\text{Al}_2\text{O}_3$  buffer layer on the growth of VACNT has also been investigated [13]. An optimum buffer layer thickness was found to minimize metal migration across the buffer layer to the silicon oxide layer and metal diffusion in the buffer layer beyond which the quantity and distribution of active catalytic particles on the surface are reduced [23,24]. Li et al. concluded that Ostwald ripening of catalyst nanoparticles, subsurface diffusion of Fe, and their activation energies for nucleation and initial growth are essential parameters for VACNT growth [25]. Growth of 2.6 mm long VACNT was achieved by reducing the catalyst at a temperature lower than the growth temperature and using low carbon feedstock to prevent carbon coating of the active catalyst [26]. Gas diffusion controls growth because the growth rate decreases with increasing CNT array length [27]. Non-uniform multiwall CNT structures 14-cm tall have been fabricated using a cold-gas CVD method [28,29] via a modified super-growth process with in situ supplementation of iron and aluminum vapor sources.

Advanced devices in medical and industrial applications, for example, those that presently utilize hollow fiber bundles, can potentially improve performance by >200–400% in key device performance parameters when substituting subcomponents that incorporate VACNTs as reactor core elements, also called fluid channel Area Bricks. Such components can be manufactured using process steps that include photolithography, electron-beam physical vapor deposition of critical thin-film catalyst multilayer stacks onto photolithographically patterned Si wafer substrates, a  $\approx$ 2-mm tall VACNT growth step inside a CVD system for such catalyst substrates followed by a few-nm-thick conformal carbon coating step, subsequent separation of the resulting precursor structures from the growth wafer, and the transformation of these precursor structures into superhydrophobic free-standing components [30–32]. The height of the components, which is dependent on the height of the related VACNT growth, is proportional to the fluid-processing capacity. Therefore, to enable the development and potential commercialization of novel VACNT-enabled applications, there is a need to develop a volume-production-scalable VACNT growth process over the total available surface area of multiple Si wafers that can produce uniform and repeatably multi-millimeter-tall 1-dimensional patterned VACNT structures with uniform spatial VACNT spacing arrangements for variously patterned layout designs that meet the targeted novel component design requirements. However, when multiple manufacturing processes that include a VACNT growth process step are combined to create novel components, the throughput, and yield of such an application-targeted VACNT growth process can fluctuate significantly owing to local height and pore size variations across one or more growth wafers, thus requiring optimization of each process step. For some of these applications, a  $\approx$  2 or 4–5-mm tall VACNT growth process that is spatially uniform and repeatable over at least one large-area substrate is key to obtaining a reasonable VACNT-enabled component production yield and increasing component value. In this paper, we present our investigation into the optimization of a modified super-growth process by optimizing the CNT catalyst design and manufacturing process, the use of an  $\text{H}_2\text{O}$  bubbler, and optimizing the CVD process for a fast VACNT growth process of >4 mm on a single 4" Si catalyst wafer. In a related paper, we investigate the benefit of using air or  $\text{O}_2$ , instead of  $\text{H}_2\text{O}$  vapor, for growing in 1.5 h uniformly > 2-mm tall VACNT forest structures on 4" Si catalyst wafers.

## 2. Materials and Methods

For all our experiments discussed here, we used a medium-sized FirstNano<sup>®</sup> EasyTube<sup>®</sup> 3000 system located in the CVD application laboratory, which is also shown in SI Figure S1. This VACNT CVD growth system had a horizontal-oriented process tube with an inner diameter of 13.1 cm, a three-zone motorized clamshell furnace, an optional 500 mL H<sub>2</sub>O bubbler, vacuum and atmospheric process capability, and an automated sample loading and offloading capability. The gases 99.99% hydrogen, ethylene, argon, and nitrogen were used as received. VACNTs synthesized using CVD on iron wafer substrates were analyzed using a Raman microscope. Raman spectra were recorded on the solid carbon nanotubes using a Raman with excitation from a 532 nm diode laser. The thickness of the catalyst and Al<sub>2</sub>O<sub>3</sub> layers was measured by a spectroscopic ellipsometer (J. A. Woollam Co., Lincoln, NE, USA). We then obtained the Delta and Psi functions which are related to the refractive index (n) and extinction coefficient (k), as well as film thickness, by fitting data to a model for films on substrates. Scanning electron microscopy was used to collect top view and cross-sectional images at varying magnifications of grown VACNTs. Thermogravimetry Differential Thermal Analysis (TG/DTA) was used to evaluate VACNT metal catalyst content. The Image J software was used to analyze the tilted view of VACNT structure and generate VACNT height profile across 4" wafer.

### 2.1. VACNT Growth Process A

The 18-mm tall VACNT's structures on a cm-sized substrate, shown in SI Figure S2, were grown on a special catalyst wafer; that is, a Si wafer with a 400-nm thick thermal oxide onto which an Al layer was first deposited by ebeam deposition. The e-beam was then vented so that the Al-thin film could be oxidized to 20 nm Al<sub>2</sub>O<sub>3</sub> using a plasma system for 10 min at 350 W, SI Figure S3. These wafers were then loaded into the same e-beam system again, and either a 1–2.5-nm Fe or 0.5/0.5-nm thick Gd/Fe layer was deposited on the top. Subsequently, the substrates were annealed in air at 400 °C. After cleaving the substrate into centimeter-sized test wafers, the test wafer was loaded into the CNT growth system. The process chamber was then evacuated to remove moisture and O<sub>2</sub> from the process tube. Subsequently, the process chamber was filled with Ar to atmospheric pressure, heated further under a constant 3000 sccm Ar flow to 600 °C, annealed for 15 min at that temperature, and then heated again under furnace temperature control until the process temperature near the test sample reached 720 °C. After switching to the cascade process temperature control mode with a process temperature target setting of 750 °C, the sample was reduced under a 100% H<sub>2</sub> flow for the next 5 min to deoxidize the thin film Fe layers. After that, for 15 h, the wafer was exposed to a mixture of 3063 sccm Ar, 1250 sccm H<sub>2</sub>, 1000 sccm C<sub>2</sub>H<sub>4</sub>, and 600 sccm Ar flowing into an H<sub>2</sub>O bubbler, which was heated to 30 °C. Cooling the wafer under Ar flow to room temperature yielded samples that were dependent on the process temperature, SI Figure S2. When the same atmospheric process was used for a full-size wafer, a VACNT with a height of approximately 1 cm was achieved using the same growth process, as shown in SI Figure S4. The top of these VACNT structures heavily curves up near their edges and becomes much denser near their top, where it is filled with amorphous carbon of approximately ~40 μm thickness. This resulted in an overall very (crusty) brittle and stiff VACNT forest structure with a non-uniform pore structure (pore size variation of over 1000% in the vertical (VACNT growth) direction); therefore, it is not suitable for highly ordered VACNT applications.

Similarly, multi-millimeter-tall single-wall VACNT structures have been grown by other authors [33] on centimeter-sized catalyst wafer samples using Fe/Gd catalyst layer(s) with thicknesses in the ranges of 0.5–1.0 nm. Some previously developed processes require a time-consuming and complex (multi-equipment) catalyst preparation process. Their maximum achievable growth height depends highly on the catalyst substrate area size, with taller structures grown on localized areas [27,28]. While FIG 2 and FIG 3 and related Figures in papers [27,28] show > cm-tall VACNT structures, their material properties were non-uniform in the vertical and horizontal directions.

## 2.2. VACNT Growth Process B

We developed a more suitable VACNT device application than Process A that generates more vertical and horizontal VACNT forests with minimal amorphous and/or polyaromatic coating covering the top level of the VACNT growth and with a pore size variation of less than 100% in the vertical direction over full-size 4" Si wafers. We accomplished this by replacing the traditionally ebeam-deposited Al film and the related plasma oxidation followed in steps from Process A with a thin Al<sub>2</sub>O<sub>3</sub> layer deposited by an ebeam on top of the thermal oxide, followed by a single thin layer of Fe in a single batch ebeam run. We used 10–30 nm Al<sub>2</sub>O<sub>3</sub> and 1–2.5 nm Fe catalyst films on a thermal oxide Si wafer substrate to grow a uniform VACNT forest over a single full 4" wafer. The carbonaceous VACNT structure was first tested by acetone soaking and subsequent evaporation, leading to a locally collapsed structure S. With this process modification, a growth time of 8 h was required with a precursor gas flow of 2775 sccm Ar, 195 sccm H<sub>2</sub>, 100 sccm C<sub>2</sub>H<sub>4</sub>, and 80 sccm Ar into the H<sub>2</sub>O bubbler heated to 30 °C to obtain an improved top-to-bottom slightly uniform multi-wall VACNT structure with a height greater than 4 mm in the center of the catalyst growth wafer, SI Figure S5, and a slightly improved top crust layer of ~20 μm thickness.

## 2.3. VACNT Growth Process C

To further accelerate the growth process, we eliminated the 15 min 600 °C catalyst film pre-annealing step from Processes A and B, and instead tested a one-step heating process from room temperature to a process thermocouple temperature of 740 °C, as fast as the system allowed (approximately 15 min) in the furnace control mode, followed by switching to cascade temperature control mode for a process temperature target of 750 °C, a 5-min H<sub>2</sub> Fe catalyst deoxidation step, a VACNT growth mode assisted by water vapor that was further optimized to the improved new catalyst process, and a cooling step to below 200 °C under a pure Ar flow. In addition to the catalyst used for Process B, a 20 nm SiO<sub>2</sub> thin film was deposited above the thermal oxide wafer before the 10 nm Al<sub>2</sub>O<sub>3</sub> film was deposited, followed by a nm-thin e-beam Fe film deposition. Finally, all three thin films were deposited in a single electron-beam batch run. The Fe film thickness was varied together with the Ar flow into the bubbler to get a 2X faster process growth from 8 h (Process B) to 4 h, and to obtain an even more uniform VACNT forest material structure with a top crust layer of about ~5–10 μm thickness.

Process C samples show similar porosity and alignment compared to samples from Process A and Process B with diameters of 8–12 nm and a spacing of 80–90 nm, SI Figure S6 and with the thinnest top "crust layer", SI Figure S7. The repeatability test was performed on Process C, and the results showed that the height varied from one run to the next by 20 %, as well as from one location to another on the same wafer, due to substrate and growth processing, SI Figure S8.

## 3. Results

Thermogravimetry-differential thermal analysis (TG-DTA) and Raman analyses were performed on the VACNT samples obtained using Process C. According to the findings presented in Figure 1a, the sample exhibited good thermal stability up to 650 °C (there was no detectable polyaromatic coating), did not contain any metal impurities that could be measured, and had an ash content that was approximately 0–1 percent. Figure 1b shows the Raman signal of the VACNT sample with a D/G ratio of approximately 1.3.

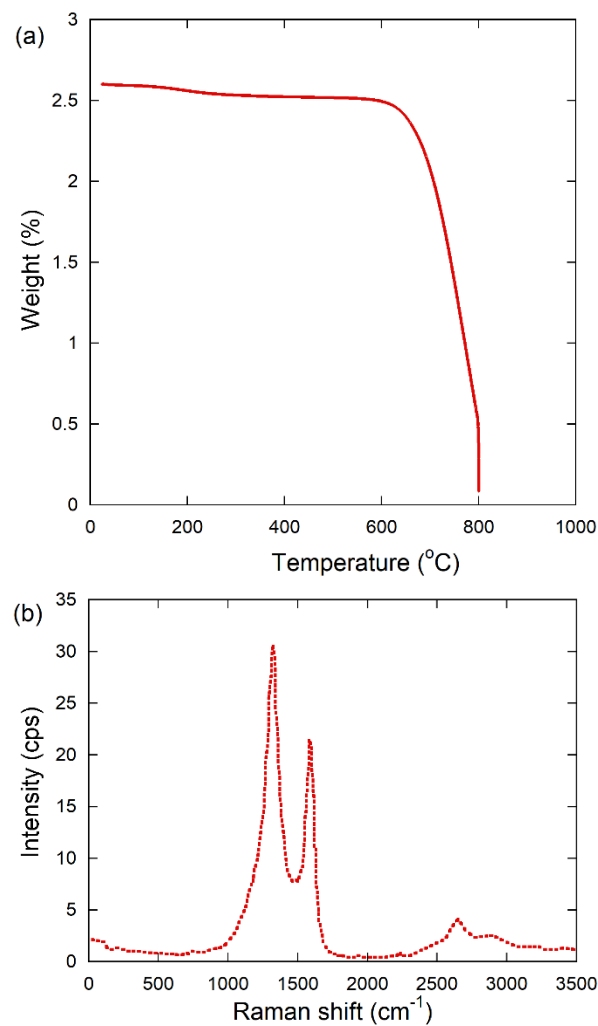


**Figure 1.** (a) TG-DTA analysis from room temperature to 800 °C, reported in weight (%) of VACNT sample grown with Process C. (b) Raman analysis of VACNT sample grown with Process C.

The reported ebeam-deposited  $\text{Al}_2\text{O}_3$  thin-film diffusion barrier from Processes B and C for Fe particles was comparable to that reported for sputtered  $\text{Al}_2\text{O}_3$  films and better than the complex and time-consuming catalyst wafer manufacturing processes used for Process A. When we tested the thickness sensitivity of the  $\text{Al}_2\text{O}_3$  thin-film layer, we found that all thicknesses  $\geq 10$  nm performed similarly and that 5 nm of the electron-beam-deposited  $\text{Al}_2\text{O}_3$  thin film reduced the growth height (catalyst lifetime) to approximately half, showing that there is a sharp threshold to a minimum thickness that sufficiently stabilized the Fe nanoparticles upon dewetting in the 5-min  $\text{H}_2$  catalyst reduction step at 740–750 °C. The next test was to replace the thermal oxide with an ebeam-deposited thin film of  $\text{SiO}_2$ , given the likely porosity of a thin  $\text{SiO}_2$  film deposited by ebeam compared to a dense 500 nm  $\text{SiO}_2$  thermal oxide diffusion barrier. However, the  $\geq 20$  nm/10 nm ebeam-deposited thin  $\text{SiO}_2/\text{Al}_2\text{O}_3$  film exhibited approximately 80% and a 500-nm thick thermal oxide film for >3–5-mm VACNT growth.

A 10 nm/10 nm  $\text{SiO}_2/\text{Al}_2\text{O}_3$  film gave only approximately half the height when growing, which would typically yield 1–2 mm tall VACNT structures, again showing a sharp barrier minimum thickness threshold, similar to the  $\text{Al}_2\text{O}_3$  film. When we combined a 500 nm  $\text{SiO}_2$  thermal oxide barrier layer with an additional 20 nm  $\text{SiO}_2$  film, the VAMWCNT growth height for a 4-h growth time was approximately 20% taller, showing that the combination of the two  $\text{SiO}_2$  layers resulted in longer life VACNT Fe catalyst particles for the Vapor Liquid Solid (VLS) VACNT growth process. This improvement was likely due to



interaction (via hydroxyl groups) between the electron-deposited  $\text{SiO}_2$  and  $\text{Al}_2\text{O}_3$  films, which further reduces the mobility of the Fe nanoparticles during VACNT growth, slowing down the related Oswald ripening effect [23] by possibly increasing the surface energy that traps the individual Fe particles locally and keeps them isolated longer, and that this thin film thickness helps with the catalytic cracking of  $\text{C}_2\text{H}_4$  in such a way that it reduces the clogging of the Fe nanoparticles with amorphous carbon during the VACNT growth phase. Eliminating any of the  $\text{Al}_2\text{O}_3$  or  $\text{SiO}_2$  barrier layers shortened the maximum-grown VACNT structures significantly. When we deposited the same 10 nm  $\text{Al}_2\text{O}_3$  film and a 1–2 nm Fe film over a copper foil, only short (typically <0.2 mm) VACNT were grown under Process C VAMWCNT process conditions. However, when we added a 20-nm  $\text{SiO}_2$  barrier layer between the Cu foil and the  $\text{Al}_2\text{O}_3$  film, greater than 1–2-mm tall VACNT forest structures can be grown.

Based on the above findings, we froze the  $\text{SiO}_2/\text{Al}_2\text{O}_3$  thin film pair to a thickness of 20 nm/10 nm for the remainder of our experiments and focused on optimizing the thickness of the Fe layer. Figure 2 shows the measured VACNT growth height for a 1.5-h growth process under the optimized conditions defined in Process C, which shows an optimum average Fe thin film layer thickness of > 1.1 nm under the tested conditions. The red line is the least-squares fit of the experimental data obtained from multiple e-beam test runs simultaneously placed in the same VAMWCNT growth CVD system batch run and from multiple repeat CVD runs with the same e-beam catalyst test samples.

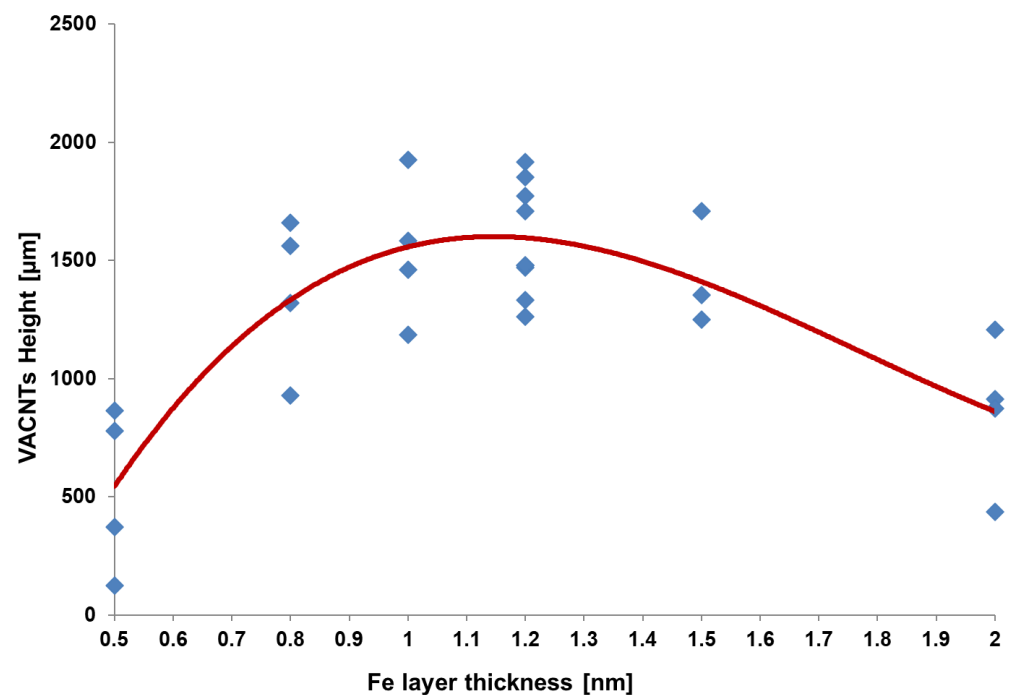


**Figure 2.** VACNT sample growth height depends on Fe layer thickness for a fixed thickness of  $\text{SiO}_2$  and  $\text{Al}_2\text{O}_3$  thin film barrier stack (Si wafer/ 20 nm  $\text{SiO}_2$ / 10 nm  $\text{Al}_2\text{O}_3$ /x nm Fe) with 90 min VACNT growth step (Process C).

Next, we varied the Ar flow into the  $\text{H}_2\text{O}$  bubbler to determine the optimum water vapor flow rate for the Process C growth condition for a 4-h VACNT growth step for the optimized catalyst sandwich layer (20 nm  $\text{SiO}_2$ /10 nm  $\text{Al}_2\text{O}_3$ /1.1 nm Fe) over a Si wafer with a 500-nm thick thermal oxide barrier layer. The observed growth height test results are summarized in Figure 3, showing an optimum rate of approximately 200 ppm partial water vapor pressure or 15 sccm Ar flow, which is lower than the 80 sccm used for Process B. Figure 2 also shows that Process C has an approximately 2× faster growth rate than Process B for a 4-mm thickness target of the VACNT structure.

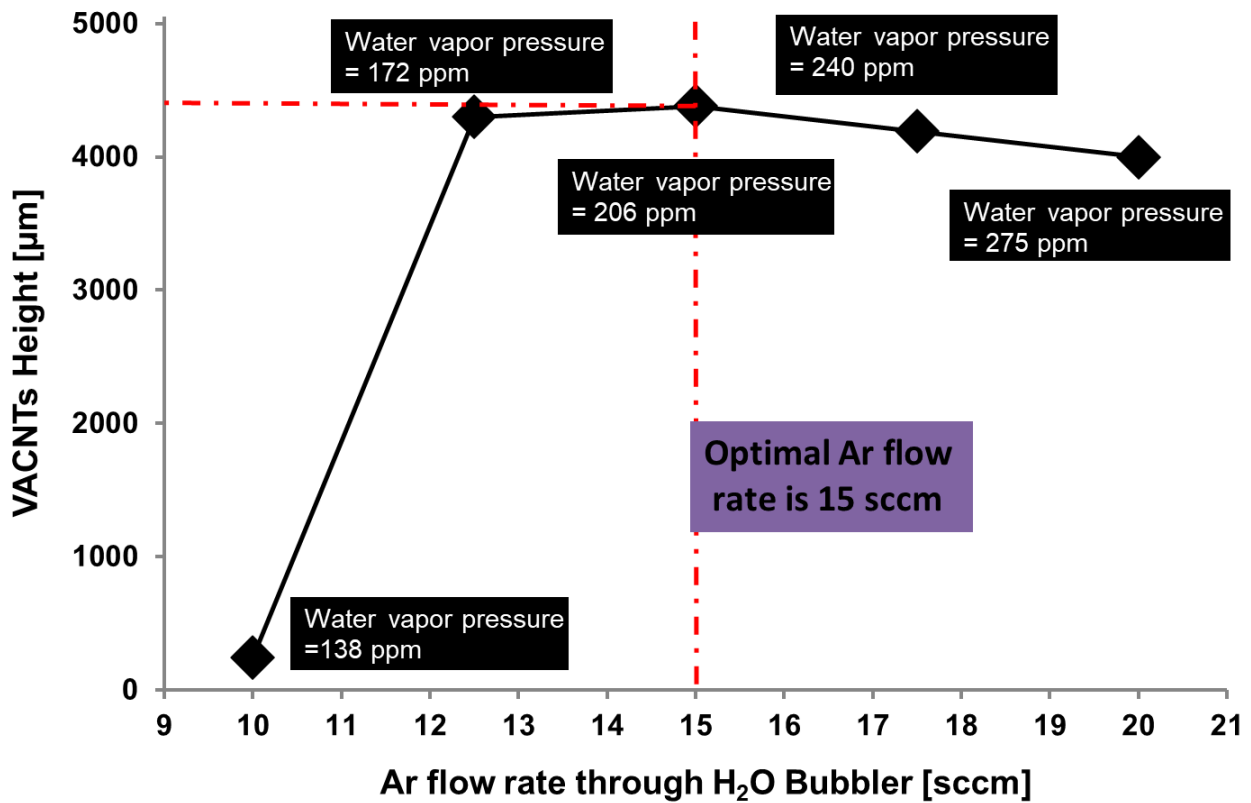


**Figure 3.** VACNT sample growth height for 4-h VACNT growth process (Process C) dependent on Ar flow into H<sub>2</sub>O bubbler for Si wafer/TO/20 nm SiO<sub>2</sub>/10 nm Al<sub>2</sub>O<sub>3</sub>/1.1 nm Fe.

Figure 4 shows a cleaved half-4" Si wafer grown as a full wafer with optimized Process C. The measured cross-sectional VACNT height profiles of the three wafers are shown in Figure 5, where all the wafer heights are higher than 4 mm; they still have a significant edge effect with the lowest growth height in the center of the wafer and a rather steep edge effect near the outer 5-mm edge of the wafer. Note that the horizontal height uniformity is still imperfect; that is, (i) it is still quite repeatable from one CNT growth run to another, and (ii) it is still improved over that of Process B and especially over Process A. Although the crust layer is not visible in Figures 4 and 5, these VACNT structures collapse after exposure to liquid acetone. In comparison to that of Process B, the crust layer of the amorphous carbon coating in Process C is notably thinner.



**Figure 4.** Tilted view of cleaved full 4" size VACNT growth wafer grown at the optimum process condition summarized as Process C.

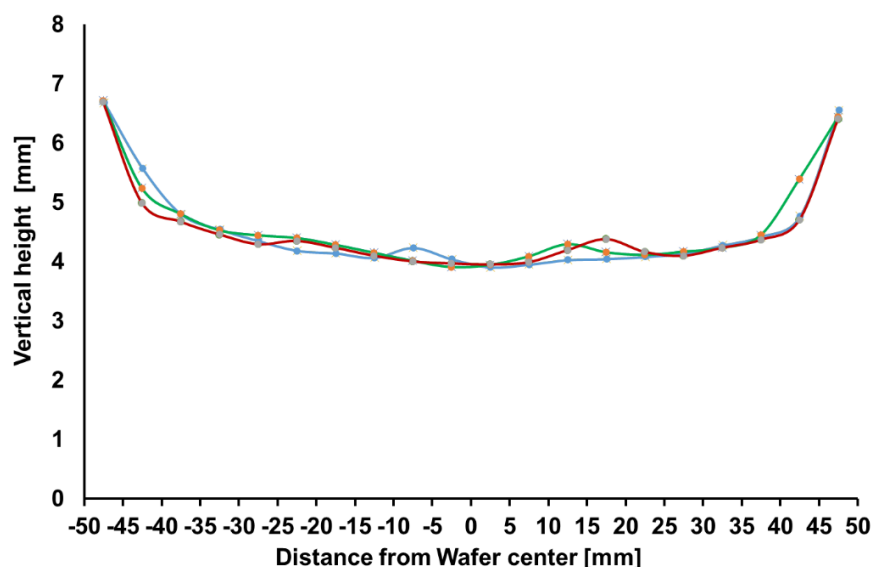


**Figure 5.** VACNT height profile across 4" wafer grown at the optimum process condition summarized as Process C.

#### 4. Conclusions

We identified a suitable catalyst growth method that was much easier and faster than process A, which was optimized for the growth of the highest VACNT structures. In particular, switching to e-beam-evaporated thin films of  $\text{SiO}_2$  and  $\text{Al}_2\text{O}_3$  helped to improve the growth height of the VACNT structures, resulting in a growth time reduction of only 4-h, combined with additional optimization of the thickness by tuning the  $\text{H}_2\text{O}$  vapor flow rate to the chosen catalyst and process growth conditions with a much simpler monolayer Fe. For growth  $>3$  mm, the combination of a thermal oxide wafer with a 20-nm  $\text{SiO}_2$  layer was optimum for growth height, whereas for structures  $<3$ -mm tall, the 20-nm  $\text{SiO}_2$  barrier layer alone was sufficient, thereby eliminating the need for thermal oxide wafers with a growth height of a few millimeters or less for most VACNT growth applications. For our modified super-growth process, the optimum water vapor concentration was approximately 200 ppm for an Fe layer thickness of approximately 1 nm. Although the change in the catalyst manufacturing process from Process A to C was successful for the tested VACNT growth system, optimal conditions of the modified catalyst manufacturing process are likely to vary depending on the structure of the reactor; therefore, reactor structure design should be considered. For instance, reactor diameter, gas residence time, reactor hot zone volume, and gas heating are crucial factors affecting heating in addition to natural convection, influencing the growth results.

Although this development was a good step toward both vertical and horizontal uniform material properties for VACNT structures over a full 4" wafer, it still shows that the horizontal height uniformity needs further improvement. While we were able to significantly improve the horizontal height uniformity by changing from Process A to Process C, further improvement with our water-based modified super-growth CNT process was halted, due to an inherent "flaw" in the water-assisted VACNT growth process for large area samples (4" or larger) that limits its horizontal growth height uniformity and leads to this characteristic water assisted "valley" height profile for larger size VACNT growth areas, and therefore, is only usable for shorter ( $<1$ – $2$  mm) and smaller size VACNT structures where subsequent height sorting is an option. In subsequent work, we will demonstrate how an optimized air- or  $\text{O}_2$ -assisted VACNT growth process can overcome the "valley" profile problem in order to process a uniform  $>2$  mm tall VACNT forest growth with very square edges and flat top surfaces on patterned 4" catalyst Si wafers. We also investigate the effects of the flow rate of air or  $\text{O}_2$  CVD precursors, the thickness of the



catalytic Fe layer, the temperature of the process growth, and the ratio of H<sub>2</sub> to C<sub>2</sub>H<sub>4</sub> on the optimal growth conditions for VACNT.

**Supplementary Materials:** The following supporting information can be downloaded at: <https://www.mdpi.com/article/10.3390/pr11061587/s1>. The supporting information contains SI Figures S1–S8.

**Author Contributions:** Conceptualization, K.S.; Methodology, K.S. and F.R.; Software, F.R.; Validation, F.R. and K.S.; Formal Analysis, K.S. and F.R.; Investigation, K.S.; Resources, K.S.; Data Curation, F.R.; Writing—Original Draft Preparation, K.S. and F.R.; Writing—Review & Editing, F.R.; Visualization, F.R.; Supervision, K.S.; Project Administration, F.R. and K.S.; Funding Acquisition, F.R. All authors have read and agreed to the published version of the manuscript.

**Funding:** The authors are thankful to the Deanship of Scientific Research at Najran University for funding this work under the Research Priorities and Najran Research funding program (NU/NRP/SERC/12/17).

**Data Availability Statement:** The data is available upon request from the corresponding author.

**Acknowledgments:** We acknowledge support from NU Labs and CVD Equipment Corporation.

**Conflicts of Interest:** The authors declare no conflict of interest.

## References

1. Takakura, A.; Beppu, K.; Nishihara, T.; Fukui, A.; Kozeki, T.; Namazu, T.; Miyauchi, Y.; Itami, K. Strength of carbon nanotubes depends on their chemical structures. *Nat. Commun.* **2019**, *10*, 3040. [CrossRef]
2. Gupta, N.; Gupta, S.M.; Sharma, S.K. Carbon nanotubes: Synthesis, properties and engineering applications. *Carbon Lett.* **2019**, *29*, 419–447. [CrossRef]
3. Yin, Z.; Wang, H.; Jian, M.; Li, Y.; Xia, K.; Zhang, M.; Wang, C.; Wang, Q.; Ma, M.; Zheng, Q.-s.; et al. Extremely Black Vertically Aligned Carbon Nanotube Arrays for Solar Steam Generation. *ACS Appl. Mater. Interfaces* **2017**, *9*, 28596–28603. [CrossRef]
4. Xu, Y.; Yan, Y.; He, T.; Zhan, K.; Yang, J.; Zhao, B.; Qi, K.; Xia, B.Y. Supercritical CO<sub>2</sub>-Assisted synthesis of NiFe<sub>2</sub>O<sub>4</sub>/vertically-aligned carbon nanotube arrays hybrid as a bifunctional electrocatalyst for efficient overall water splitting. *Carbon* **2019**, *145*, 201–208. [CrossRef]
5. Fedorovskaya, E.O.; Bulusheva, L.G.; Kurennya, A.G.; Asanov, I.P.; Rudina, N.A.; Funtov, K.O.; Lyubutin, I.S.; Okotrub, A.V. Supercapacitor performance of vertically aligned multiwall carbon nanotubes produced by aerosol-assisted CCVD method. *Electrochim. Acta* **2014**, *139*, 165–172. [CrossRef]
6. Trivedi, S.; Alameh, K. Effect of vertically aligned carbon nanotube density on the water flux and salt rejection in desalination membranes. *SpringerPlus* **2016**, *5*, 1158. [CrossRef]
7. Pinheiro, R.A.; Rosa, F.M.; Volú, R.M.; de Vasconcelos, G.; Trava-Airoldi, V.J.; Corat, E.J. Vertically aligned carbon nanotubes (VACNT) surfaces coated with polyethylene for enhanced dew harvesting. *Diam. Relat. Mater.* **2020**, *107*, 107837. [CrossRef]
8. Pinheiro, R.A.; Damm, D.D.; Silva, A.A.; Volu, R.M.; Almeida, K.F.; Rosa, F.M.; Trava-Airoldi, V.J.; Corat, E.J. Water Vapor Condensation from Atmospheric Air by Super-Hydrophobic VACNTs Growth on Stainless Steel Pipes. *MRS Adv.* **2019**, *4*, 1929–1936. [CrossRef]
9. Rana, M.; Asyraf, M.R.M. Investigation and development of vertically aligned carbon nanotube (VACNT) forest based temperature sensor. *Microelectron. Eng.* **2016**, *162*, 93–95. [CrossRef]
10. Machado, G.; Coelho, C. Vertically-aligned carbon nanotube at low pressure by cold-wall thermal CVD using a two-phase deposition step. *Carbon Trends* **2021**, *5*, 100087. [CrossRef]
11. Shoukat, R.; Khan, M.I. Carbon nanotubes: A review on properties, synthesis methods and applications in micro and nanotechnology. *Microsyst. Technol.* **2021**, *27*, 4183–4192. [CrossRef]
12. Cao, T.T.; Nguyen, V.C.; Ngo, T.T.T.; Le, T.L.; Nguyen, T.L.; Tran, D.L.; Obratzsova, E.D.; Phan, N.M. Effects of ferrite catalyst concentration and water vapor on growth of vertically aligned carbon nanotube. *Adv. Nat. Sci. Nanosci. Nanotechnol.* **2014**, *5*, 045009. [CrossRef]
13. Noda, S.; Hasegawa, K.; Sugime, H.; Kakehi, K.; Zhang, Z.; Maruyama, S.; Yamaguchi, Y. Millimeter-Thick Single-Walled Carbon Nanotube Forests: Hidden Role of Catalyst Support. *Jpn. J. Appl. Phys.* **2007**, *46*, L399–L401. [CrossRef]
14. Ohashi, F.; Chen, G.Y.; Stolojan, V.; Silva, S.R.P. Influences of hydrogen gas on carbon nanotube growth. *MRS Online Proc. Libr. (OPL)* **2008**, *1081*, 87–93. [CrossRef]
15. Hata, K.; Futaba Don, N.; Mizuno, K.; Namai, T.; Yumura, M.; Iijima, S. Water-Assisted Highly Efficient Synthesis of Impurity-Free Single-Walled Carbon Nanotubes. *Science* **2004**, *306*, 1362–1364. [CrossRef]
16. Liu, H.; Zhang, Y.; Li, R.; Sun, X.; Wang, F.; Ding, Z.; Mérel, P.; Desilets, S. Aligned synthesis of multi-walled carbon nanotubes with high purity by aerosol assisted chemical vapor deposition: Effect of water vapor. *Appl. Surf. Sci.* **2010**, *256*, 4692–4696. [CrossRef]
17. Futaba, D.N.; Hata, K.; Yamada, T.; Mizuno, K.; Yumura, M.; Iijima, S. Kinetics of Water-Assisted Single-Walled Carbon Nanotube Synthesis Revealed by a Time-Evolution Analysis. *Phys. Rev. Lett.* **2005**, *95*, 056104. [CrossRef]

18. Amama, P.B.; Pint, C.L.; Kim, S.M.; McJilton, L.; Eyink, K.G.; Stach, E.A.; Hauge, R.H.; Maruyama, B. Influence of Alumina Type on the Evolution and Activity of Alumina-Supported Fe Catalysts in Single-Walled Carbon Nanotube Carpet Growth. *ACS Nano* **2010**, *4*, 895–904. [[CrossRef](#)]
19. Liu, Q.; Shi, X.; Jiang, Q.; Li, R.; Zhong, S.; Zhang, R. Growth mechanism and kinetics of vertically aligned carbon nanotube arrays. *EcoMat* **2021**, *3*, e12118. [[CrossRef](#)]
20. Brukh, R.; Mitra, S. Mechanism of carbon nanotube growth by CVD. *Chem. Phys. Lett.* **2006**, *424*, 126–132. [[CrossRef](#)]
21. Kumar, M.; Ando, Y. Chemical Vapor Deposition of Carbon Nanotubes: A Review on Growth Mechanism and Mass Production. *J. Nanosci. Nanotechnol.* **2010**, *10*, 3739–3758. [[CrossRef](#)]
22. Xie, K.; Muhler, M.; Xia, W. Influence of water on the initial growth rate of carbon nanotubes from ethylene over a cobalt-based catalyst. *Ind. Eng. Chem. Res.* **2013**, *52*, 14081–14088. [[CrossRef](#)]
23. Sakurai, S.; Nishino, H.; Futaba, D.N.; Yasuda, S.; Yamada, T.; Maigne, A.; Matsuo, Y.; Nakamura, E.; Yumura, M.; Hata, K. Role of Subsurface Diffusion and Ostwald Ripening in Catalyst Formation for Single-Walled Carbon Nanotube Forest Growth. *J. Am. Chem. Soc.* **2012**, *134*, 2148–2153. [[CrossRef](#)]
24. Hasegawa, K.; Noda, S. Moderating carbon supply and suppressing Ostwald ripening of catalyst particles to produce 4.5-mm-tall single-walled carbon nanotube forests. *Carbon* **2011**, *49*, 4497–4504. [[CrossRef](#)]
25. Li, H.; Yuan, G.; Shan, B.; Zhang, X.; Ma, H.; Tian, Y.; Lu, H.; Liu, J. Chemical Vapor Deposition of Vertically Aligned Carbon Nanotube Arrays: Critical Effects of Oxide Buffer Layers. *Nanoscale Res. Lett.* **2019**, *14*, 106. [[CrossRef](#)]
26. Gul, O.T. A simple method to grow millimeters long vertically aligned carbon nanotube forests. *Diam. Relat. Mater.* **2021**, *120*, 108637. [[CrossRef](#)]
27. Cho, W.; Schulz, M.; Shanov, V. Kinetics of growing centimeter long carbon nanotube arrays. In *Syntheses and Applications of Carbon Nanotubes and Their Composites*; IntechOpen: Rijeka, Croatia, 2013. [[CrossRef](#)]
28. Cho, W.; Schulz, M.; Shanov, V. Growth and characterization of vertically aligned centimeter long CNT arrays. *Carbon* **2014**, *72*, 264–273. [[CrossRef](#)]
29. Sugime, H.; Sato, T.; Nakagawa, R.; Hayashi, T.; Inoue, Y.; Noda, S. Ultra-long carbon nanotube forest via in situ supplements of iron and aluminum vapor sources. *Carbon* **2021**, *172*, 772–780. [[CrossRef](#)]
30. Fazio, W.C.; Lund, J.M.; Wood, T.S.; Jensen, B.D.; Davis, R.C.; Vanfleet, R.R. Material Properties of Carbon-Infiltrated Carbon Nanotube-Templated Structures for Microfabrication of Compliant Mechanisms. In *Proceedings of the ASME 2011 International Mechanical Engineering Congress and Exposition 2011, Volume 11: Nano and Micro Materials, Devices and Systems; Microsystems Integration*, Denver, CO, USA, 11–17 November 2011; pp. 481–490. [[CrossRef](#)]
31. Strobl, K.; Gainey, S.; Kesich, M.; Brogan, J.; Kumar, A. *Fluid Reactor and Fluid Reactor Component Manufacturing*; World International Property Organization: Geneva, Switzerland, 2021; Volume 046394, pp. 1–96.
32. Strobl, K.; Gainey, S.; Kumar, A. *Fluid Reactors*; World International Property Organization: Geneva, Switzerland, 2020; Volume 092816, pp. 1–148.
33. Sugime, H.; Sato, T.; Nakagawa, R.; Cepek, C.; Noda, S. Gd-enhanced growth of multi-millimeter-tall forests of single-wall carbon nanotubes. *ACS Nano* **2019**, *13*, 13208–13216. [[CrossRef](#)]

**Disclaimer/Publisher’s Note:** The statements, opinions and data contained in all publications are solely those of the individual author(s) and contributor(s) and not of MDPI and/or the editor(s). MDPI and/or the editor(s) disclaim responsibility for any injury to people or property resulting from any ideas, methods, instructions or products referred to in the content.